Journal of Molecular Liquids 375 (2023) 121366

Contents lists available at ScienceDirect

Journal of Molecular Liquids

journal homepage: www.elsevier.com/locate/molliq

Nitrate adsorption using green iron oxide nanoparticles synthesized by Eucalyptus leaf extracts: Kinetics and effects of pH, KCl salt, and anions competition

Ehsan Khoshkalam [a], Amir Fotovat [a,*], Akram Halajnia [a], Hossein Kazemian [b,c], Hossein Eshghi [d]

[a] Department of Soil Science, Faculty of Agriculture, Ferdowsi University of Mashhad (FUM), Mashhad, Iran
[b] Northern Analytical Laboratory Services (NALS), Northern BC's Environment and Climate Solutions Innovation Hub, University of Northern British Columbia (UNBC), Prince George, BC, Canada
[c] Chemistry Department, Faculty of Science and Engineering, University of Northern British Columbia, Prince George, BC, Canada
[d] Department of Chemistry, Faculty of Sciences, Ferdowsi University of Mashhad (FUM), Mashhad, Iran

ARTICLE INFO

Article history:
Received 24 October 2022
Revised 18 January 2023
Accepted 29 January 2023
Available online 31 January 2023

Keywords:
Adsorption
Agglomeration
Engineered nanoparticles
Green chemistry
Mechanism
Water pollution

ABSTRACT

This research investigated the colloidal stability and reactivity of green iron oxide nanoparticles for removing NO_3^- ions from polluted water. These nanoparticles were synthesized by Eucalyptus *globulus* leaf extract (EL-Fe NPs). Transmission electron microscopy (TEM), energy-dispersive X-ray spectroscopy (EDS), X-ray diffraction (XRD), Fourier-transform infrared spectroscopy (FT-IR), and dynamic light scattering (DLS) were utilized to characterize EL-Fe NPs. The effect of contact time, different pH, KCl salt, and anions (PO_4^{3-}, SO_4^{2-}, HCO_3^-, Cl^-), on NO_3^- adsorption using EL-Fe NPs were evaluated. Based on the results, Fe_3O_4 and α-Fe_2O_3 nanoparticles were encapsulated by polyphenols and have irregular nanoparticulate structures. After 30 min, the maximum adsorption capacity of 1.5 g L^{-1} EL-Fe NPs dispersed in 50 mg L^{-1} NO_3^- solution with a pH of 3.7 was acquired at about 12.91 mg/g. Adsorption of NO_3^- on EL-Fe NPs was strongly pH dependent, and at pH > 6.6 no significant adsorption occurred. KCl salt by agglomeration of EL-Fe NPs, the mean particle size varied between 25.6 nm and 63 nm, and NO_3^- adsorption decreased dramatically. It was observed that EL-Fe NPs significant affinity to adsorb PO_4^{3-} ions. As a result, no significant adsorption of NO_3^- ions onto EL-Fe NPs was detected in the presence of phosphate ions. The experimental data were reasonably fit to a pseudo-second-order kinetic model (R^2 = 0.992), which can be concluded that the primary mechanism of NO_3^- adsorption is electrostatic. This work indicated that the removal of NO_3^- using EL-Fe NPs was influenced by the type and concentration of accompanying cations and anions.

1. Introduction

Chemical fertilizers, domestic and industrial wastewaters, waste leachate, etc. are important sources of NO_3^- pollutant [1]. Nitrate enters the aquatic ecosystem easily due to its high solubility in water and its lack of adsorption by the soil. The maximum permissible concentration of nitrate in drinking water is 50 mg L^{-1} [2,3]. A High NO_3^- concentrations harms the environment, humans, and animals [3,4]. For instance, the existence of NO_3^- in aquatic phase progresses the eutrophication and likewise creates methemoglobinemia disease for human while intake the drinking water along with NO_3^- species [3,8]. Therefore, it is necessary to remove or reduce its concentration in the environment [5]. During the last decades, various techniques such as adsorption, Ion exchange, reverse osmosis, chemical reduction, biological denitrification, and more were used for NO_3^- removal from water [2,3,6-9]. Application of these techniques has some drawbacks including difficulty to operation, high costs, producing sludge, short lifespan, low efficiency, and high energy consumption [3,4]. For example, the biological approach is time-consuming and produces biological sludge. Also, some methods such as chemical reduction could produce harmful by-products during the decontamination process [3,8].

Among all approaches, due to cost-effective and high efficiency, the adsorption-based techniques have gained more attention among researchers. So far, various materials and compounds have been used to adsorb NO_3^-. These materials include biochar

* Corresponding author.
E-mail addresses: e.khoshkalam@mail.um.ac.ir (E. Khoshkalam), afotovat@um.ac.ir (A. Fotovat), halajnia@um.ac.ir (A. Halajnia), hossein.kazemian@unbc.ca (H. Kazemian), heshghi@um.ac.ir (H. Eshghi).

https://doi.org/10.1016/j.molliq.2023.121366
0167-7322/

[1,10,11], clays [5,12], LDH [13,14], iron nanoparticles [15], graphene [16], activated carbon [17], alumina magnetic hybrid nanoparticles [3] Fe_3O_4@GelHT composite [18], (Fe_3O_4)/alginate (Alg) (MAlg) composite [7], and more. However, iron oxide (hydroxide) nanoparticles are one of the most favored adsorbents for environmental applications due to the high efficiency of these particles in removing pollutants and their eco-friendliness compared to other metal nanoparticles [19]. Furthermore, iron oxide (hydroxide) nanoparticles have an excellent regeneration ability, therefore, the overall cost of adsorbents will be reduced [6,18]. Nonetheless, the synthesis and use of these materials have their challenges. In the synthesizing process, iron oxide (hydroxide) nanoparticles tend to agglomerate due to the predominance of magnetic and van der Waals forces. Furthermore, using hazardous substances to synthesis nanoparticles may harm the environment [20-24].

Due to such issues, the usage of green chemical technology in the environment has achieved global acceptance in recent years [19]. This technology synthesizes metal nanoparticles such as iron, copper, gold, silver, and other metals by using plant-based products or microorganisms as starting materials [19,20]. For instance, plant and microbial-produced polyphenols play the role of capping and stabilizing agents [19]. Therefore, production costs are significantly reduced, and no harmful material enters the environment during the synthesis and utilization of nanoparticles [25]. In addition, due to the capping and stabilization of nanoparticles by polyphenols, metal nanoparticles agglomerate to a small degree owing to the surface charge [20,21,24]. So far, extracts of green tea [20,22,26], Eucalyptus [23,24,27-29], Moringa oleifera [4], Murrayakoenigii leaves [30], and other plant extracts have been used to synthesize iron oxide (hydroxide) nanoparticles. Numerous studies reported the use of these particles for the removal of different contaminants such as heavy metals [31-33], dyes [22,26,28], and phosphate from the environmental matrix [34].

Nevertheless, some research has been done on NO_3^- adsorption by iron nanoparticles produced using green chemistry method [4,27]. The reaction mechanism and stability of iron oxide (hydroxide) nanoparticles synthesized by green chemistry for NO_3^- adsorption are relatively unknown. Indeed, adsorption reactions could be impacted by several factors including acidity, surface charge density and hydration radius of cations and anions, specific or non-specific reaction between adsorbent and adsorbates, and hydrophilic or hydrophobic nature of adsorbent [35-38].

Coating and stabilizing iron oxides (hydroxides) with organic compounds, such as polyphenolic substances, could change particles surface charge and hydrophobicity [39]. On the other hand, some studies argued that the solution chemistry can affect surface charge and agglomeration/dispersion of colloidal particles [35,37]. For example, previous study reported decreasing surface charge and agglomeration of magnetite nanoparticles coated with citric acid (CA-MNPs) in the presence of Na^+ and Ca^{2+} cations [39]. Oncsik et al. [35] investigated the effect of monovalent salts such as $N(CH_3)_4Cl$, NH_4Cl, CsCl, KCl, NaCl, and LiCl on the charge variation and agglomeration of polystyrene latex particles. They observed as the concentration of each of these salts increased, the agglomeration of the particles increased. In another research, the negative charge of silica particles decreased with increasing concentrations of NaCl, KCl, and CsCl, [36]. Battas et al. [5] used a clay mineral as a NO_3^- adsorbent where NO_3^- adsorption decreased with increasing particle size and decreasing effective specific surface area.

Eucalyptus has been utilized to synthesize iron oxide nanoparticles (EL-Fe NPs) for the removal of various contaminants including NO_3^- ions [23,24,27-29,34]. However, the adsorption of NO_3^- by EL-Fe NPs in environmental matrices and varying media solution pH is not studied thoroughly. Therefore, for a better understanding of the effect of the solution chemistry on the NO_3^- adsorption by EL-Fe NPs, the role of KCl concentrations, as a media solution, on zeta potential, agglomeration, and NO_3^- adsorption capacity of EL-Fe NPs was evaluated. While inquiring about the reaction kinetics, the effect of pH and other competing anions on NO_3^- adsorption was studied.

2. Materials and methods

2.1. Materials and reagents

Analytical grade Iron(III) chloride hexahydrate ($FeCl_3{\cdot}6H_2O$, 99 %), sodium nitrate ($NaNO_3$, 99.5 %), potassium chloride (KCl, 99.5 %), sodium hydroxide (NaOH, 98 %), potassium sulfate (K_2SO_4, 99 %), potassium dihydrogen phosphate (KH_2PO_4, 99.5 %), and Sodium hydrogen carbonate ($NaHCO_3$, 99.5 %) were purchased from Merck, Germany. All chemicals were used as received. Eucalyptus extract was made from *Eucalyptus globulus* leaves obtained from a local store.

2.2. Preparation of EL-Fe NPs

Fig. 1 Shows the steps for synthesizing of EL-Fe NPs. In a typical extraction experiment, 50 g of Eucalyptus leaves were added to 1L deionized water and heated at 80 °C for 1 h. After cooling to room temperature, the extract was vacuum filtred [27,40]. To synthesize EL-Fe NPs, a 0.1 M ferric iron solution ($FeCl_3{\cdot}6H_2O$) was added to the Eucalyptus leaves extract at a 1:2 v/v ratio [4,32] and stirred for 1 h [21]. The synthesized Fe NP was separated from the supernatant by centrifugation at 10000 rpm (30 min) and washed with deionized water (3 times). The sample was identified as EL-Fe NPs and stored in a refrigerator at 4 °C.

2.3. Characterization of EL-Fe NPs

Field emission scanning electron microscopy (FESEM, LMU TESCAN BRNO-MIRA3, Czech Republic) was utilized to investigate the morphology of EL-FeNPs. Transmission electron microscopy examined the samples' structure and particle size (TEM). TEM images were acquired with a LEO0912 AB (ZEISS-Germany) electron microscope set to 160 kV and a point-to-point resolution of 1.9 A. To prepare the TEM sample, a droplet of the EL-Fe NPs suspension (in water) was placed on a copper grid with a holey carbon film and dried under vacuum at room temperature. The sample chemical composition was measured using EDS data collected by an SEM-EDS instrument (LEO1450vp, ZEISS, Germany).

The structure and crystallinity of the nanoparticles were also assessed by X-ray diffraction (XRD), using an X-ray diffractometer (GNR instrument, Explorer, Italy) equipped with Cu Kα radiation (λ = 1.54 Å) source. The sample was processed within the 2θ range of 10 – 80°. FT-IR spectrometer (Thermo Nicolet, AVATAR 370 FT-IR, USA) was used to study the functional groups on the surface of iron oxide nanoparticles. For FT-IR measurement, the EL-Fe NPs suspension was freeze-dried. The obtained powder was mixed with 100 mg of KBr powder at 1 % (w/w) and pressed into a thin slice. An average of 32 scans with a resolution of 2 cm^{-1} were collected for each measurement. A Cordouan, Vasco3, France analyzed mean particle size and distribution. The CAD, Zeta Compact, France was used for determining the zeta potential of iron oxide nanoparticles. Ultraviolet–Visible Spectroscopy (UV–Vis, Dynamica HALO XB-10, UK) was applied to measure the residual concentration of the NO_3^- during the adsorption process.

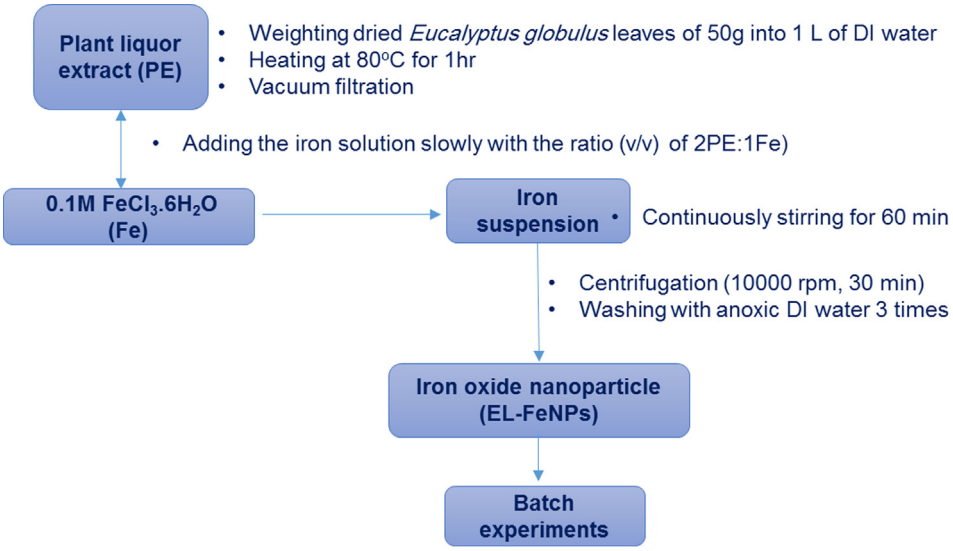

Fig. 1. Flowchart of synthesizing iron oxide nanoparticles using Eucalyptus *globulus* leaf extracts.

2.4. NO_3^- adsorption

2.4.1. Effect of contact time and equilibrium pH

The experiments were carried out in 50 ml glass vials. In a typical adsorption test, 15 mg EL-FeNPs were added to 10 ml solutions with the Initial NO_3^- concentration of 50 mg L^{-1} (without adjusting pH), which was prepared using a 1000 mg L^{-1} stock solution, to determine the equilibrium time. The mixture was agitated on the shaker at 250 rpm for desired time (e.g. 5–120 min). Then, the mixture was centrifuged at 13000 rpm for 10 min, to separate the adsorbent and supernatant. The equilibrium pH was measured in the supernatant solutions. The concentration of equilibrium NO_3^- was measured using a UV–vis spectrophotometer (Dynamica HALO XB-10) at a wavelength of 220 nm. To correct the errors associated with organic matter in the solution, the samples were also measured at 275 nm [27]. All experiments were carried out in duplicate. NO_3^- adsorption in percent (R%) and q_t (mg g^{-1}) was obtained using equations (1) and (2), respectively [5,41,42].

$$R(\%) = \frac{C_0 - C_t}{C_0} \times 100 \quad (1)$$

$$q_t = \frac{(C_0 - C_t)V}{W} \quad (2)$$

Where C_0 (mg L^{-1}) and C_t (mg L^{-1}) are the residual concentration of NO_3^- at 0 and t (min) reaction time, respectively, V (L) is the volume of the solution and W (g) is the mass of the EL-Fe NPs used. For determining the optimal pH of the reaction, different amounts of sodium hydroxide (0.1 M) were added to the reaction mixture containing 1.5 g L^{-1} of EL-Fe NPs and 50 mg L^{-1} of NO_3^-.

2.4.2. Kinetic study

To determine the maximum amount of adsorbed NO_3^- and to identify the reaction control step, three different kinetic models were employed including the pseudo-first-order (Equation (3)), pseudo-second-order (Equation (4)), and intraparticle diffusion (Equation (5)) model [14,42]. To obtain information about the equilibrium adsorption capacity of adsorbents, pseudo-first-order and pseudo-second-order models are typically used, and the model with the highest correlation coefficient is applied to determine the adsorption capacity. The intraparticle diffusion model also determines whether or not intraparticle diffusion is rate-limiting.

$$\log(q_e - q_t) = \log q_e - \log\left(\frac{k_1 t}{2.303}\right) \quad (3)$$

$$\frac{t}{q_t} = \frac{1}{k_2 q_e^2} + \frac{t}{q_e} \quad (4)$$

$$q_t = k_p t^{1/2} + C \quad (5)$$

In these equations, q_t, q_e, K_1, K_2, K_p, C, and t are respectively the amount of ion adsorbed at time t (mg g^{-1}), the amount of ion adsorbed at equilibrium time (mg g^{-1}), pseudo-first-order rate constant (min^{-1}), pseudo-second-order rate constant (mg min^{-1}), interparticle diffusion rate constant (mg g^{-1} min^{-1}), intercept and time (min).

2.4.3. Effect of KCl on NO_3^- adsorption

The effect of KCl salt on NO_3^- adsorption and particle stability was studied. In a typical experiment, EL-Fe Nps (15 mg) were added to 10 ml solutions containing 50 mg L^{-1} NO_3^- and different concentrations of KCl (0 to 100 mM). After shaking the solution (250 rpm) at the equilibrium time, NO_3^- concentration, zeta potential, and mean particle size were measured.

2.4.4. Effect of anions on NO_3^- adsorption

To study the impact of competing anion on NO_3^- adsorption, the 10 ml solution containing anions ($[NO_3^-]$, $[PO_4^{3-}]$, $[SO_4^{2-}]$, $[HCO_3^-]$, and $[Cl^-]$ = 0.8 mmol L^{-1}) were prepared in 1 mM KCl. 15 mg of nanoparticles was added to the solution and agitated for 30 min at 250 rpm, then centrifuged. The equilibrium pH was recorded and concentrations of NO_3^- [27], PO_4^{3-} [43], and SO_4^{2-} [44] were measured. Concentrations of HCO_3^- and Cl^- were measured using the titrimetric method [45].

3. Results and discussion

3.1. Characterization

3.1.1. XRd

The X-ray diffraction (XRD) pattern of iron oxide nanoparticles is presented in Fig. 2**.** The XRD pattern shows a broad hump which is characteristic of an amorphous structure. The broad peak at 2θ = 26.64 could be attributed to the presence of organic matter

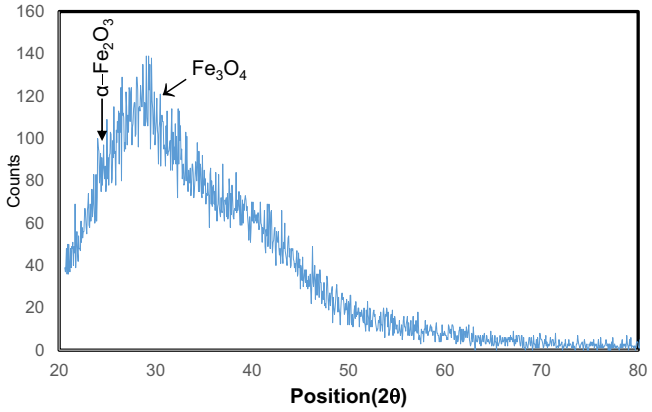

Fig. 2. X-ray diffraction (XRD) pattern of EL-Fe NPs.

and indicate that the polyphenols obtained from *E. globulus* extract could act as a capping and stabilizing agent for iron oxide nanoparticles, which was approved by following FTIR results [4,24]. In addition, the slight peaks at around 2θ of 24.26 and 30.49 could be corresponded to α-Fe_2O_3 and Fe_3O_4, respectively. Some recent studies also mentioned the presence of iron oxides in Eucalyptus extract [23,24,27,46].

3.1.2. FTIR analysis

Fig. 3. exhibits FTIR spectra of fresh and spent EL-Fe NPs. In fresh sorbent, the broadband peak at 3406 cm^{-1} is related to the stretching vibration of O—H [28,29,47]. The adsorption peaks in the range of 1400 cm^{-1} and 1622 cm^{-1} could be attributed to the stretching vibrations of the C—C bond in alkenes and benzene rings [29]. The peak at 1068 cm^{-1} indicates the stretching vibrations of the C═C bond [28]. The absorption band at 1713 cm^{-1} could be ascribed to carbonyl groups from aliphatic acids [27]. Bands at 447 cm^{-1} and 518 cm^{-1} could be associated with Fe—O stretching vibrations of hematite and magnetite nanoparticles [24,27]. After the adsorption process, most of the FTIR bands of EL-FeNPs were shifted in FTIR spectra, which confirms NO_3^- adsorption. Adsorption of NO_3^-, remarkably reduced the intensity of —OH groups proving the interaction of NO_3^- anions with surface functional groups of EL-FeNPs. Moreover, the appearance of the intense band around 1382 cm^{-1} indicates the existence of the N—O bonds caused from NO_3^- adsorption [3].

3.1.3. FESEM, TEM micrograph, EDS and DLS analysis

The FESEM image of EL-FeNPs (Fig. 4.a) is evident that particles appear spherical and uniform in size along with slight agglomeration. Fig. 4.b shows the structure and size of EL-Fe Nps agglomerates obtained by transmission electron microscopy. According to the TEM image, after the reaction between *Eucalyptus* extract and $FeCl_3$ solution, Fe NPs encapsulated by polyphenol have irregular nanoparticulate structures, which is consistent with those reported in the literature [20,21].

According to the SEM-EDS data (Fig. 4.c), the EL-Fe Nps consisted of Fe (13.3 %), O (40.1 %), C (44.3 %), and P (1.9 %). Prominent peaks for oxygen and carbon were related to biomolecules of *Eucalyptus* leaf extract and also oxygen indicating the presence of iron oxide in EL-Fe NPs [24,27].

DLS was employed to determine the average particle size and polydispersity index (PDI). The results showed that the *Eucalyptus globulus* leaf extract was able to produce nanoparticles with an average size of 25.6 nm (Fig. 4.d). Also, the PDI was 0.1503 confirming that the suspension was homogenous [4,48]. The obtained nanoparticles are smaller in size and more homogenous compared to previous research [4,39] Moreover, the average zeta potential of nanoparticles was −32.54 mV. Such a zeta potential indicates that eucalyptus leaf extract has coated iron oxide nanoparticles well and the nanoparticles are stable [39,48].

3.2. Kinetic study of NO_3^- adsorption

The effect of contact time on NO_3^- adsorption capacity is shown in Fig. 5. Nitrate adsorption on the Fe-oxide nanoparticles appeared to be instant and more than 8.6 mg g^{-1} (approx.. 67 % of total adsorbed) of NO_3^- was absorbed within the first 10 min of the reaction. Moreover, equilibrium was reached within 30 min of the reaction, with no further significant adsorption observed. The fast adsorption of NO_3^- by EL-FeNPs could be related to their structure and high surface area. Polyphenolic compounds could act as capping and stabilizing agents. By coating the surface of iron oxide nanoparticles, the number of active adsorption sites for NO_3^- has increased. Therefore, the reaction kinetics is very high. The decrease in reaction rate from the initial 10 min to the equilibrium point was probably related to the diffusion of NO_3^- into the EL-Fe

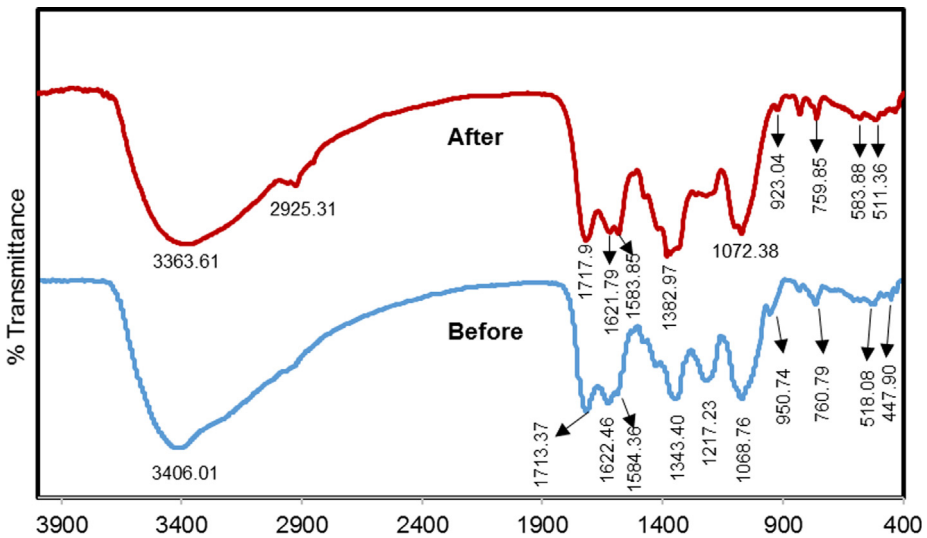

Fig. 3. Fourier-transform infrared spectroscopy (FT-IR) spectra of fresh and spent EL-Fe NPs.

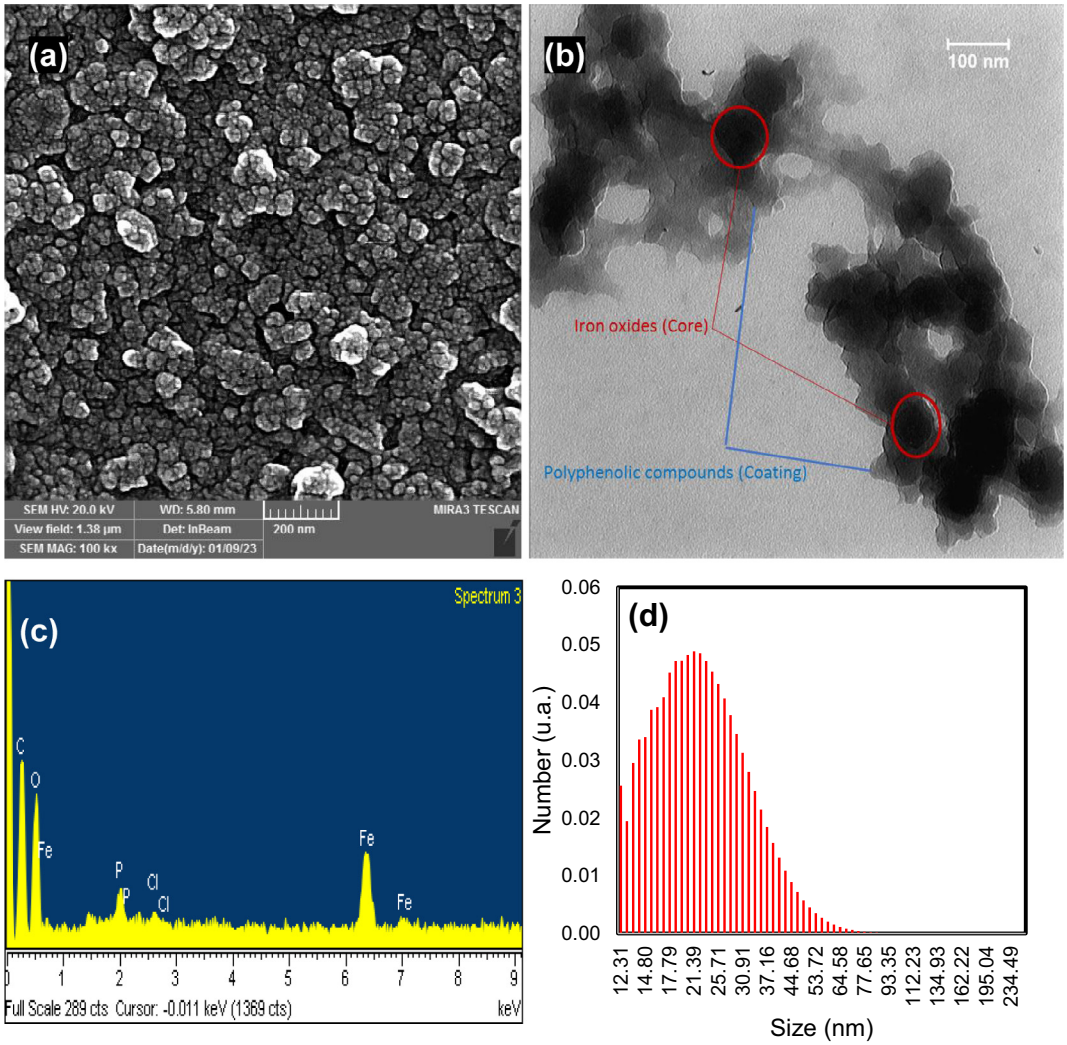

Fig. 4. FESEM (a), TEM micrograph (b), EDS analysis (c), and mean particle size by dynamic light scattering (DLS) (d) of EL-FeNPs.

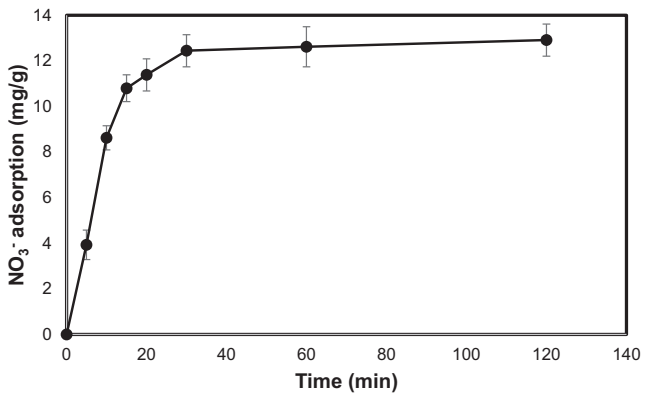

Fig. 5. Nitrate adsorption by EL-Fe NPs as a function of shaking time ([EL-Fe NPs] = 1.5 g L^{-1}, [NO_3^-] = 50 mg L^{-1}, pHe ≈ 3.7, room temperature).

NPs. This result was obtained while the equilibrium pH was 3.7. At acidic pH, NO_3^- is electrostatically adsorbed by protonation of the surface functional groups of EL-FeNPs. Therefore, this type of adsorption can be considered a reason for the rapid reaction [16,27,49].

Pseudo-first-order, pseudo-second-order, and intra-particle diffusion kinetic models were applied to fit the experimental data. The parameters can be seen in Table 1. The pseudo-second-order model fits more appropriately with the experimental results. The pseudo-first-order model had a lower amount of determination coefficient (R^2) than the pseudo-second-order model. Also, the $q_{e.cal}$ obtained by the pseudo-first-order was lesser than the $q_{e.cal}$ acquired by the pseudo-second-order. The intraparticle diffusion model with a correlation coefficient of 0.613 cannot be used to describe NO_3^- absorption data. In contrast, the $q_{e.cal}$ obtained by the pseudo-second-order model was very close to the $q_{e.exp}$ obtained from the analysis of laboratory data (Table 1). In addition, the high determination coefficient of the pseudo-second-order (0.992) shows that NO_3^- absorption by EL-FeNPs follows the pseudo-second-order kinetic equation. Similar findings have been reported in the literature for iron nanoparticles synthesized by Eucalyptus extract [27] and other adsorbents such as Mg-Fe LDH [14], amine cross-linked tea wastes (ACTW) [49], and graphene [16].

3.3. Effect of pH

The efficiency of EL-Fe NPs in NO_3^- adsorption was evaluated at different equilibrium pH (Fig. 6). According to the results, the highest NO_3^- adsorption occurred in acidic pH values. So, with the gradual increase of pH from 3.7 to about 6, the amount of adsorption dramatically decreased from about 40 to 6.6 %. At a pH higher than

Table 1
Kinetic parameters for NO_3^- adsorption on EL-Fe NPs.

	Pseudo-first-order			Pseudo-second-order			Intraparticle diffusion		
$q_{e.exp}$	$q_{e.cal}$ (mg g^{-1})	K_1 (min^{-1})	R^2	$q_{e.cal}$ (mg g^{-1})	K_2 (g min^{-1} min^{-1})	R^2	C	K_p (mg g^{-1} $min^{-1/2}$)	R^2
12.91	8.198	0.067	0.964	13.477	0.016	0.992	3.6868	1.1396	0.613

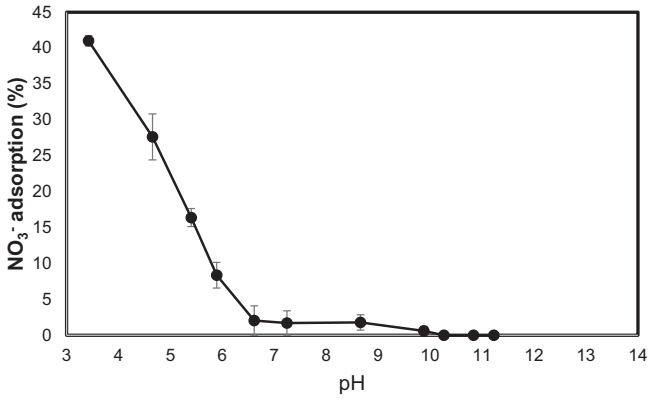

Fig. 6. The effect of equilibrium pH on NO_3^- adsorption ([EL-Fe NPs] = 1.5 g L^{-1}, [NO_3^-] = 50 mg L^{-1}, Shaking time = 30 min, room temperature).

6.65, no significant adsorption of NO_3^- was observed. By coating iron oxide nanoparticles with eucalyptus polyphenols, NO_3^- adsorption sites can be divided into two groups: 1) adsorption active sites derived from eucalyptus polyphenols (gallic acid, ellagic acid, hydrolyzable tannins, leuco anthocyanins, and flavonol glycosides)[23,27], and 2) adsorption sites of iron oxide nanoparticles α-Fe_2O_3 and Fe_3O_4, which have 4–10 iron-hydroxyl group bonds per square nanometer and show amphoteric behavior [11]. At acidic pHs, the adsorption sites produced by polyphenols are coordinated by H^+ ions resulting in a positive surface charge which can adsorb NO_3^-. With increasing pH, surface functional groups are deprotonated, and on the other hand, OH^- ions compete with NO_3^- for the adsorption sites leading to the dominance of OH^- ions on the adsorption sites [49,50]. In the case of α-Fe_2O_3 and Fe_3O_4 nanoparticles NO_3^- can be adsorbed via an electrostatic and ligand exchange [51]. Because of the factors mentioned above and the increased of the electrostatic repulsion force between the surface of particles and the NO_3^- ion, adsorption decreases dramatically [1,5,10,11]. In similar research, where NO_3^- adsorption was done with activated carbon, NO_3^- adsorption efficiency decreased drastically with increasing pH [12,50].

3.4. Mechanism of NO_3^- adsorption

As discussed earlier, two kinds of mechanisms can be ascribed to NO_3^- adsorption by EL-Fe NPs: electrostatic attraction and ligand exchange. In this system, the highest amount of adsorption occurred in acidic conditions (Fig. 6). Indeed, the acidity of the solution plays an essential role in controlling adsorption process. Therefore, it can be concluded that due to the protonation of functional groups of EL-Fe NPs and creation of positive surface charge, the main mechanism is electrostatic attraction [1,10,51]. The abundance of functional groups in the FT-IR spectrum also confirms this issue. Electrostatic attraction mechanism indicated in Eq. (6–8).

$$\equiv FeOH + H^+ \leftrightarrow \equiv FeOH_2^+ \quad (6)$$

$$\equiv FeOH_2^+ + NO_3^- \leftrightarrow \equiv FeOH_2^+ \ldots NO_3^- \quad (7)$$

$$\equiv FeOH - Ar - OH_2^+ + NO_3^- \leftrightarrow \equiv FeOH - Ar - OH_2^+ \ldots NO_3^- \quad (8)$$

Here, $-Ar - OH_2^+$ indicate the polyphenolic compounds that coated iron oxides.

On the other hand, some studies argued that NO_3^- can be adsorbed via ligand exchange by Fe and Al oxides [3,51]. Under acidic conditions, it is possible to adsorb NO_3^- in the form of bidentate binuclear (BB) and monodentate mononuclear (MM) by hydrated iron oxides [51]. In the MM situation, NO_3^- binding to one H_2O surface functional group with one OH group in the adjacent surface sites of iron oxides. BB and MM mechanisms are indicated in Eq. (9) and Eq. (10) respectively [51].

$$[Fe_2(OH)_4(H_2O)_6.(H_2O)_6]^{2+} + NO_3^- \leftrightarrow [Fe_2(OH)_4(H_2O)_4NO_3.(H_2O)_6]^{+1} \quad (9)$$

$$[Fe_2(OH)_5(H_2O)_5.(H_2O)_6]^{+} + NO_3^- \leftrightarrow [Fe_2(OH)_5(H_2O)_4NO_3.(H_2O)_6]^{0} \quad (10)$$

Of course, all suggested mechanisms are relatively weak under basic conditions [51]. Schematic illustration (Fig. 7) was proposed to clarify the NO_3^- adsorption mechanisms using EL-Fe NPs.

3.5. Effects of KCl concentration on the NO_3^- adsorption and aggregation of EL-Fe NPs

Fig. 8.a. shows the effect of KCl concentration on NO_3^- adsorption at a pHe ≈ 3.7. With increasing KCl concentration, NO_3^- adsorption was decreased, so that, in the 0, 1, 10, and 100 mM KCl, the adsorption rate was 12.17, 7.32, 4.24, and 0.15 mg g^{-1}, respectively. Most likely, the reduction of NO_3^- adsorption can be explained using the results of Fig. 8.b. In Fig. 8.b, the accumulation of EL-Fe NPs particles in the presence of NO_3^- ions and different KCl concentrations were measured using DLS. The effect of KCl and NO_3^- on the zeta potential of EL-Fe NPs was investigated. The zeta potential of EL-Fe NPs did not change drastically in the presence of NO_3^- and KCl salt and only slightly decreased in high concentrations of KCl. However, their effects on particle size are quite evident. So that by adding NO_3^- ions (50 mg L^{-1}) to EL-Fe NPs suspension, the average particle size increased from 25.62 to 36.89 nm. Adding KCl to the suspension containing EL-Fe NPs and NO_3^- affected the particle size significantly. Hence, the high concentration of potassium chloride (100 mM) changed the average particle size of EL-Fe NPs to more than 63 nm. The change in EL-Fe NPs particle sizes can be well explained by referring to the Hofmeister series and DLVO theory.

Based on the Hofmeister series, potassium and NO_3^- have the can agglomerate and change colloidal particles stability [35,36]. DLVO theory also attributes the stability or lack of stability of colloidal particles to the dominance of electrostatic repulsion forces and Van der Waals forces [35-39,52].Therefore, as mentioned earlier, in acidic pHs the functional groups of EL-Fe NPs are protonated. As a result, with NO_3^- adsorption, the electrostatic repulsion of the particles and the thickness of the electrical double layer (EDL) are reduced, and agglomeration occurs. By adding KCl salt, potassium is adsorbed by EL-Fe NPs. Although the adsorption of potassium had a negligible effect on the zeta potential of

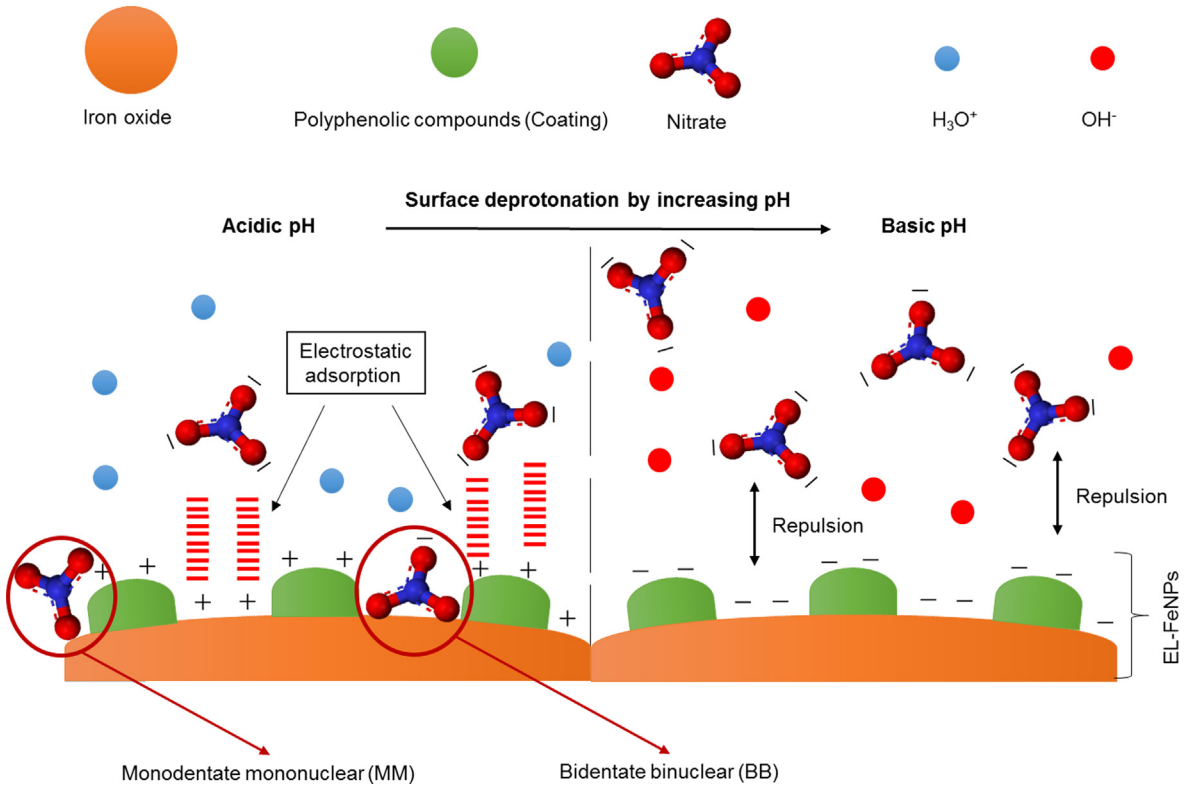

Fig. 7. The proposed mechanisms of nitrate adsorption by EL-Fe NPs.

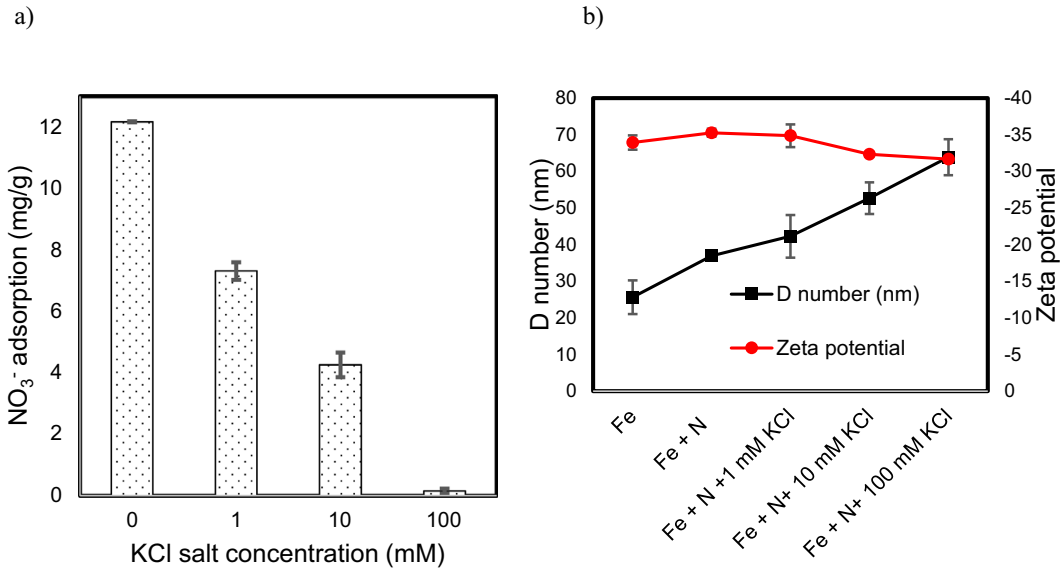

Fig. 8. a) The effect of KCl concentration on NO_3^- adsorption by EL-FeNPs, b) The effect of NO_3^- and KCl on zeta potential and aggregation of EL-FeNPs (Fe = EL-FeNPs, N = NO_3^-, [EL-FeNPs] = 1.5 g L^{-1}, [NO_3^-] = 50 mg L^{-1}, pHeq ≈ 3.7, shaking time = 30 min, and room temperature).

nanoparticles, it has caused the size of EL-Fe NPs to increase. Thus, potassium significantly affects coagulation and reduces particles' stability [36,37,52]. Increasing the particle size means the effective specific surface area of the particles is reduced [5,36], and the significant decrease in NO_3^- adsorption is probably related to this issue. A schematic of the effect of KCl salt on NO_3^- adsorption and aggregation of EL-Fe NPs is illustrated in Fig. 9. Indeed, electrostatic adsorption is more affected by the concentration of the media solution [53]. Therefore, According to the experimental results (see Fig. 8), it can be argued that the primary mechanism of NO_3^- adsorption is electrostatic.

Besides investigating the effect of KCl concentration on particle aggregation, the effect of solution pH in this reaction should not be ignored. The pH of solutions affects the critical coagulation concentration (CCC) of colloidal particles. According to research, particle coagulation occurs in low concentrations of monovalent salts in acidic pH. As the pH increases, due to the deprotonation of functional groups and the increase in the negative charge of the surface,

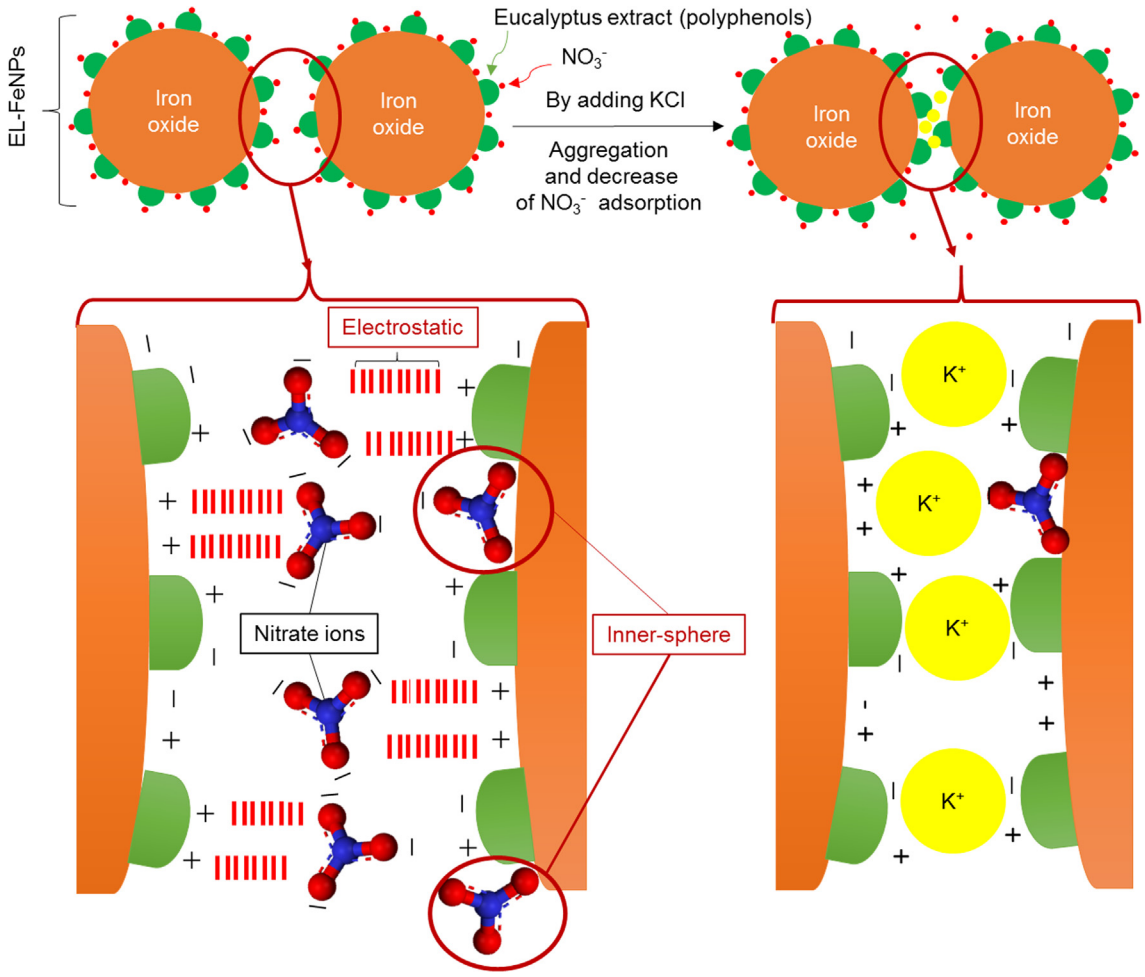

Fig. 9. Schematic illustration of the effect of KCl salt on NO_3^- adsorption and aggregation of EL-Fe NPs.

higher concentrations of monovalent salts are needed to aggregate the particles [39,54]. The effect of pH on the coagulation of magnetite nanoparticles coated with citric acid (CA-MNPs) in the presence of NaCl was reported [39]. The CCC of CA-MNPs particles at pH 5, 7, and 9 were 25.06, 92.83, and 438.9 mM NaCl, respectively. Our experimental results indicated that at a pH of 3.7, even low concentrations of KCl could cause aggregation of EL-Fe NPs particles. On the other hand, chloride ions compete with NO_3^- ions for EL-Fe NPs adsorption sites, which could be contributed to the reduced nitrate adsorption [17,41].

3.6. The effect of competing anions

The effect of PO_4^{3-}, HCO_3, SO_4^{2-}, and Cl^- anions (with the same concentration of 0.8 mmol/L) on NO_3^- adsorption by EL-Fe NPs was investigated. At the equilibration (i.e. 30 min) and an equilibrium pH of 4, no measurable NO_3^- adsorption was observed. Meanwhile, from other anions in the solution, only phosphate ion was adsorbed (%75.32) by EL-Fe NPs. The explanations for this reaction could be related to 1) the surface characteristics of EL-Fe NPs, 2) the competition of phosphate ions with other anions for the adsorption sites, and 3) the type of phosphate species in the solution. The phosphate adsorption mechanism is summarized in three forms electrostatic adsorption, ion exchange, and Lewis acid-base reaction [55]. According to the XRD and FTIR results, the dominant type of iron oxides in EL-FeNPs was α-Fe_2O_3 and Fe_3O_4 (Fig. 2 and Fig. 3). Experimental data showed that the ZPC of α-Fe_2O_3 varies between 7 and 9.2 and of Fe_3O_4 is about 8 [54], which means α-Fe_2O_3 and Fe_3O_4 nanoparticles have a positive surface charge in a wide range of pH ($pH < pH_{zpc}$) [54]. The dominant phosphate species at equilibrium pH 4 is $H_2PO_4^-$ [56]. $H_2PO_4^-$ competes with other anions for the adsorption sites and is electrostatically adsorbed by the protonation of functional groups on the surface of polyphenols and iron oxides [57].

On the other hand, iron oxide nanoparticles α-Fe_2O_3 and Fe_3O_4 have a strong tendency to adsorb phosphate ions. One of the reactions between phosphate and α-Fe_2O_3 and Fe_3O_4 is through ion exchange [57]. During the ligands exchange between the hydroxyl ion of iron oxide nanoparticles and the phosphate ion, phosphate is adsorbed, and the hydroxyl ion is released into the solution. Also, during the Lewis acid-base reaction, the active sites of α-Fe_2O_3 and Fe_3O_4 act as the Lewis base, while the phosphate ion acts as the Lewis acid. As a result, iron oxide particles form bonds with phosphate oxygen ions, Fe-O bonds are formed, and water molecules are released into the solution [57]. Consequently, based on the below equations, phosphate ions compete with other anions for the adsorption sites, either electrostatically or in the form of ion exchange reactions and Lewis acid-base, and the negative charge of the surface increases with the adsorption of phosphate [56,57].

$$\equiv FeOH + H^+ \leftrightarrow \equiv FeOH_2^+ \quad (11)$$

$$\equiv FeOH_2^+ + H_2PO_4^- \leftrightarrow \equiv FeOH_2^+ \ldots H_2PO_4^- \quad (12)$$

Table 2
Comparison of EL- Fe NPs with other adsorbents in NO_3^- adsorption.

Materials	NO_3^- adsorption capacity (mg g^{-1})	pH	Equilibrium time (min)	References
Metal modified biochar	32.33	≈ 4	300	[10]
Mg–Fe LDH biochar	24.8	–	300	[13]
Graphene	89.97	7	45	[16]
α-Fe2O3 and Fe3O4 dispersed on Douglas fir biochar	15	2	10	[11]
Amine-crosslinked tea waste (ACTW)	136.43	3–10	10	[49]
Activated Carbon	9.8	3	360	[50]
Local clay	1.54	2	120	[5]
Sepiolite activated by HC	10	2–10	5	[12]
Mg-Fe-LDH	18.5	7	30	[14]
AMH nanosorbent	69	6	80	[3]
Fe_3O_4	2.37	5	40	[9]
AFMCS composite beads	38.40	5	30	[9]
EL-Fe NPs	9.698	5.7	60	[27]
EL-Fe NPs	12.91	3.7	30	Current study

$$\equiv FeOH + H_2PO_4^- \leftrightarrow \equiv FePO_4^{2-} + H^+ + H_2O \quad (13)$$

$$\equiv FeOH + H_2PO_4^- \leftrightarrow \equiv FePO_4H^- + H_2O \quad (14)$$

$$\equiv FeOH + H_2PO_4^- + H^+ \leftrightarrow \equiv FePO_4H_2^0 + H_2O \quad (15)$$

By occupying the adsorption sites with phosphate ions, the adsorbent's surface's negative charge will increase, leading to electrostatic repulsion between the EL-Fe NPs and anions in the solution. Thus, the adsorption of other anions such as NO_3^- will be significantly reduced. Iida et al. [50] studied NO_3^- adsorption by activated carbon and concluded that the presence of phosphate and sulfate anions effectively reduces NO_3^- adsorption. Some studies found that the presence of accompanying anions not only does not affect the adsorption of phosphate but even increases the amount of phosphate adsorption [57,58]. In research, phosphate adsorption slightly increased by increasing the anions of NO_3^-, sulfate, and chloride in the solution from 0 to 50 mg L^{-1} [57]. Also, Lǔ et al. [58] showed no change in phosphate adsorption with increasing ionic strength and the presence of HCO_3^- and SO_4^{2-} anions. Therefore, it is concluded that due to the inner-sphere reaction of phosphate with iron oxide nanoparticles, the amount of adsorption is less affected by the ionic strength and the increased concentration of accompanying anions [59]. As a result, other anions such as NO_3^-, are not adsorbed by EL-Fe NPs.

3.7. Comparative studies

The maximum NO_3^- adsorption capacity by EL-Fe NPs was compared to that of other NO_3^- adsorbents previously reported in the literature (Table 2). The adsorption capacity of EL-Fe NPs is higher than in the previous study, which used eucalyptus extract [27], and also similar to or more than other sorbents such as Activated Carbon [50], Fe_3O_4 [9], Local clay [5], and Sepiolite activated by HCl [12]. Of course, this study's adsorption capacity is lower than Mg-Fe-LDH [14], Metal modified biochar [10], Mg-Fe LDH biochar [13], Graphene [16], Amine-crosslinked tea waste (ACTW) [49], AMH nonosorbent [3], and AFMCS composite bead [9]. Nevertheless, it seems that the synthesis of EL-Fe NPs is eco-friendly, economical, and much more straightforward. The maximum NO_3^- adsorption capacity by EL-FeNPs, similar to other adsorbents with similar chemical properties, was obtained in acidic conditions. Equilibration time is a significant factor that can be used for the feasibility of using an adsorbent for the purification process. Table 2 shows EL-Fe NPs have a very short equilibrium time compared to most sorbents. Because the efficiency of EL-Fe NPs in NO_3^- adsorption decreases with increasing ionic strength, it can be used as a promising material for NO_3^- removal, provided the structure of EL-FeNPs is modified.

4. Conclusion

Using *Eucalyptus globulus* leaf extract, Fe_3O_4 and α-Fe_2O_3 nanoparticles were successfully synthesized and used for nitrate adsorption from contaminated water. The experimental data depicted that the solution chemistry can affect the colloidal stability and NO_3^- removal efficiency. The outline of the acquired results are as follows: (1) Acidic pH (≈3.7) was the most favorable for NO_3^- adsorption (≈40 %). In the basic pH, by deprotonation of surface functional groups, competition of OH^- ions, and increasing electrostatic force repulsion on the surface of EL-Fe NPs, no significant adsorption of NO_3^- occurred (2) Ion exchange and electrostatic attraction can be the main mechanisms of NO_3^- adsorption in acidic pH. (3) EL-Fe NPs were agglomerated in the presence of KCl salt and the average particle size, more than 145 %, was increased. Consequently, because of the reduced specific surface area of EL-Fe NPs, NO_3^- adsorption at about 98 % decreased. (4) EL-Fe NPs had a strong affinity to adsorb phosphate ions. As a result, by adsorbing phosphate and increasing the surface's negative charge, no significant adsorption of NO_3^- occurred. In general, the data presented in the current study implies that green synthesized nanoparticles might apply to the aquatic and terrestrial environment for the decontamination of NO_3^-.

Data availability

Data will be made available on request.

Declaration of Competing Interest

The authors declare that they have no known competing financial interests or personal relationships that could have appeared to influence the work reported in this paper.

Acknowledgments

This work was supported by the Ferdowsi University of Mashhad, Mashhad, Iran (grant No. 45893).

References

[1] M. Zhang, G. Song, D.L. Gelardi, L. Huang, E. Khan, Evaluating biochar and its modifications for the removal of ammonium, nitrate, and phosphate in water, Water Res. J. 186 (2020), https://doi.org/10.1016/j.watres.2020.116303.
[2] I. Aswin Kumar, A. Jeyaseelan, N. Viswanathan, M. Naushad, A.J.M. Valente, Fabrication of lanthanum linked trimesic acid as porous metal organic frameworks for effective nitrate and phosphate adsorption, J. Solid State Chem. 302 (2021), https://doi.org/10.1016/j.jssc.2021.122446.
[3] Z. Karimi, A. Rahbar-Kelishami, Preparation of highly efficient and eco-friendly alumina magnetic hybrid nanosorbent from red mud: Excellent adsorption

capacity towards nitrate, J. Mol. Liq. 368 (2022), https://doi.org/10.1016/j.molliq.2022.120751.
[4] L. Katata-Seru, T. Moremedi, O.S. Aremu, I. Bahadur, Green synthesis of iron nanoparticles using Moringa oleifera extracts and their applications: Removal of nitrate from water and antibacterial activity against Escherichia coli, J. Mol. Liq. 256 (2018) 296–304, https://doi.org/10.1016/j.molliq.2017.11.093.
[5] A. Battas, A. el Gaidoumi, A. Ksakas, A. Kherbeche, Adsorption study for the removal of nitrate from water using local clay, Sci. World J. 2019 (2019), https://doi.org/10.1155/2019/9529618.
[6] I. Aswin Kumar, N. Viswanathan, Hydrothermal Fabrication of Amine-Grafted Magnetic Gelatin Hybrid Composite for Effective Adsorption of Nitrate and Phosphate, Ind. Eng. Chem. Res. 58 (2019) 21521–21530, https://doi.org/10.1021/acs.iecr.9b04815.
[7] I.A. Kumar, N. Viswanathan, Micro-encapsulation and hydrothermal tuning of amine decorated magnetic alginate hybrid beads for nitrate and phosphate remediation, J. Taiwan Inst. Chem. Eng. 102 (2019) 283–296, https://doi.org/10.1016/j.jtice.2019.06.017.
[8] I.A. Kumar, A. Jeyaseelan, S. Ansar, N. Viswanathan, A facile synthesis of 2D iron bridged trimesic acid based MOFs for superior nitrate and phosphate retention, J. Environ. Chem. Eng. 10 (2022), https://doi.org/10.1016/j.jece.2022.107233.
[9] I. Aswin Kumar, N. Viswanathan, Development and Reuse of Amine-Grafted Chitosan Hybrid Beads in the Retention of Nitrate and Phosphate, J. Chem. Eng. Data 63 (2018) 147–158, https://doi.org/10.1021/acs.jced.7b00751.
[10] L. Long, Y. Xue, X. Hu, Y. Zhu, Study on the influence of surface potential on the nitrate adsorption capacity of metal modified biochar, Environmental Science and Pollution, Research 26 (2019) 3065–3074, https://doi.org/10.1007/s11356-018-3815-z.
[11] N. Bombuwala, A.S. Liyanage, C.U. Pittman, D. Mohan, T. MIsna, Bioresource Technology Fast nitrate and fl uoride adsorption and magnetic separation from water on α -Fe 2 O 3 and Fe 3 O 4 dispersed on Douglas fi r biochar, Bioresour. Technol. 263 (2018) 258–265, https://doi.org/10.1016/j.biortech.2018.05.001.
[12] N. Öztürk, T.E. Bektaş, Nitrate removal from aqueous solution by adsorption onto various materials, J. Hazard. Mater. 112 (2004) 155–162, https://doi.org/10.1016/j.jhazmat.2004.05.001.
[13] L. Xue, B. Gao, Y. Wan, J. Fang, S. Wang, Y. Li, R. Muñoz-Carpena, L. Yang, High efficiency and selectivity of MgFe-LDH modified wheat-straw biochar in the removal of nitrate from aqueous solutions, J. Taiwan Inst. Chem. Eng. 63 (2016) 312–317, https://doi.org/10.1016/j.jtice.2016.03.021.
[14] A. Halajnia, S. Oustan, N. Najafi, A.R. Khataee, A. Lakzian, The adsorption characteristics of nitrate on Mg-Fe and Mg-Al layered double hydroxides in a simulated soil solution, Appl. Clay Sci. 70 (2012) 28–36, https://doi.org/10.1016/j.clay.2012.09.007.
[15] Y. Liu, J. Wang, Reduction of nitrate by zero valent iron (ZVI)-based materials: A review, Sci. Total Environ. 671 (2019) 388–403, https://doi.org/10.1016/j.scitotenv.2019.03.317.
[16] P. Ganesan, R. Kamaraj, S. Vasudevan, Journal of the Taiwan Institute of Chemical Engineers Application of isotherm, kinetic and thermodynamic models for the adsorption of nitrate ions on graphene from aqueous solution, J. Taiwan Inst. Chem. Eng. (2013) 1–7, https://doi.org/10.1016/j.jtice.2013.01.029.
[17] K. Ota, Y. Amano, M. Aikawa, M. Machida, Removal of nitrate ions from water by activated carbons (ACs) - Influence of surface chemistry of ACs and coexisting chloride and sulfate ions, Appl. Surf. Sci. 276 (2013) 838–842, https://doi.org/10.1016/j.apsusc.2013.03.053.
[18] I.A. Kumar, N. Viswanathan, A facile synthesis of magnetic particles sprayed gelatin embedded hydrotalcite composite for effective phosphate sorption, J. Environ. Chem. Eng. 6 (2018) 208–217, https://doi.org/10.1016/j.jece.2017.11.042.
[19] P. Mondal, A. Anweshan, M.K. Purkait, Green synthesis and environmental application of iron-based nanomaterials and nanocomposite: A review, Chemosphere 259 (2020), https://doi.org/10.1016/j.chemosphere.2020.127509.
[20] P. Plachtová, Z. Medříková, R. Zbořil, J. Tuček, R.S. Varma, B. Maršálek, Iron and Iron Oxide Nanoparticles Synthesized with Green Tea Extract: Differences in Ecotoxicological Profile and Ability to Degrade Malachite Green, ACS Sustain. Chem. Eng. 6 (2018) 8679–8687, https://doi.org/10.1021/acssuschemeng.8b00986.
[21] Z. Markova, P. Novak, J. Kaslik, P. Plachtova, M. Brazdova, D. Jancula, K.M. Siskova, L. Machala, B. Marsalek, R. Zboril, R. Varma, Iron(II,III)-polyphenol complex nanoparticles derived from green tea with remarkable ecotoxicological impact, in: ACS Sustain Chem Eng, American Chemical Society, 2014: pp. 1674–1680. https://doi.org/10.1021/sc5001435.
[22] R. Abbassi, A.K. Yadav, N. Kumar, S. Huang, P.R. Jaffe, Modeling and optimization of dye removal using "green" clay supported iron nanoparticles, Ecol. Eng. 61 (2013) 366–370, https://doi.org/10.1016/j.ecoleng.2013.09.040.
[23] M. Martínez-Cabanas, M. López-García, J.L. Barriada, R. Herrero, M.E. Sastre de Vicente, Green synthesis of iron oxide nanoparticles. Development of magnetic hybrid materials for efficient As(V) removal, Chem. Eng. J. 301 (2016) 83–91, https://doi.org/10.1016/j.cej.2016.04.149.
[24] T. Wang, X. Jin, Z. Chen, M. Megharaj, R. Naidu, Science of the Total Environment Green synthesis of Fe nanoparticles using eucalyptus leaf extracts for treatment of eutrophic wastewater, Sci. Total Environ. 466–467 (2014) 210–213, https://doi.org/10.1016/j.scitotenv.2013.07.022.
[25] M. Nasrollahzadeh, M. Sajjadi, S. Iravani, R.S. Varma, Green-synthesized nanocatalysts and nanomaterials for water treatment: Current challenges and future perspectives, J. Hazard. Mater. 401 (2021), https://doi.org/10.1016/j.jhazmat.2020.123401.
[26] K.K. Singh, K.K. Senapati, K.C. Sarma, Synthesis of superparamagnetic Fe3O4 nanoparticles coated with green tea polyphenols and their use for removal of dye pollutant from aqueous solution, J. Environ. Chem. Eng. 5 (2017) 2214–2221, https://doi.org/10.1016/j.jece.2017.04.022.
[27] T. Wang, J. Lin, Z. Chen, M. Megharaj, R. Naidu, Green synthesized iron nanoparticles by green tea and eucalyptus leaves extracts used for removal of nitrate in aqueous solution, J. Clean. Prod. 83 (2014) 413–419, https://doi.org/10.1016/j.jclepro.2014.07.006.
[28] Z. Wang, C. Fang, M. Megharaj, Characterization of iron-polyphenol nanoparticles synthesized by three plant extracts and their fenton oxidation of azo dye, ACS Sustain. Chem. Eng. 2 (2014) 1022–1025, https://doi.org/10.1021/sc500021n.
[29] Z. Wang, C. Yu, C. Fang, M. Mallavarapu, Dye removal using iron-polyphenol complex nanoparticles synthesized by plant leaves, Environ. Technol. Innov. 1–2 (2014) 29–34, https://doi.org/10.1016/j.eti.2014.08.003.
[30] C. Prasad, P. Krishna Murthy, R.H. Hari Krishna, R. Sreenivasa Rao, V. Suneetha, P. Venkateswarlu, Bio-inspired green synthesis of RGO/Fe3O4 magnetic nanoparticles using Murrayakoenigii leaves extract and its application for removal of Pb(II) from aqueous solution, J. Environ. Chem. Eng. 5 (2017) 4374–4380, https://doi.org/10.1016/j.jece.2017.07.026.
[31] D. Mukherjee, S. Ghosh, S. Majumdar, K. Annapurna, Green synthesis of α-Fe2O3 nanoparticles for arsenic(V) remediation with a novel aspect for sludge management, J. Environ. Chem. Eng. 4 (2016) 639–650, https://doi.org/10.1016/j.jece.2015.12.010.
[32] C. Mystrioti, T.D. Xanthopoulou, P.E. Tsakiridis, N. Papassiopi, A. Xenidis, Comparative evaluation of five plant extracts and juices for nanoiron synthesis and application for hexavalent chromium reduction, Sci. Total Environ. 539 (2016) 105–113, https://doi.org/10.1016/j.scitotenv.2015.08.091.
[33] C. Prasad, K. Sreenivasulu, S. Gangadhara, P. Venkateswarlu, Bio inspired green synthesis of Ni/Fe3O4magnetic nanoparticles using Moringa oleifera leaves extract: A magnetically recoverable catalyst for organic dye degradation in aqueous solution, J. Alloy. Compd. 700 (2017) 252–258, https://doi.org/10.1016/j.jallcom.2016.12.363.
[34] Q. Xu, W. Li, L. Ma, D. Cao, G. Owens, Z. Chen, Simultaneous removal of ammonia and phosphate using green synthesized iron oxide nanoparticles dispersed onto zeolite, Sci. Total Environ. 703 (2020), https://doi.org/10.1016/j.scitotenv.2019.135002.
[35] T. Oncsik, G. Trefalt, M. Borkovec, I. Szilagyi, Specific ion effects on particle aggregation induced by monovalent salts within the Hofmeister series, Langmuir 31 (2015) 3799–3807, https://doi.org/10.1021/acs.langmuir.5b00225.
[36] M. Dishon, O. Zohar, U. Sivan, From repulsion to attraction and back to repulsion: The effect of NaCl, KCl, and CsCl on the force between silica surfaces in aqueous solution, Langmuir 25 (2009) 2831–2836, https://doi.org/10.1021/la803022b.
[37] H. Mateos, R.A. Picca, A. Mallardi, M. Dell'Aglio, A. de Giacomo, N. Cioffi, G. Palazzo, Effect of the surface chemical composition and of added metal cation concentration on the stability of metal nanoparticles synthesized by pulsed laser ablation in water, Appl. Sci. (Switzerland). 10 (2020) 1–12, https://doi.org/10.3390/APP10124169.
[38] N. Schwierz, D. Horinek, R.R. Netz, Anionic and cationic hofmeister effects on hydrophobic and hydrophilic surfaces, Langmuir 29 (2013) 2602–2614, https://doi.org/10.1021/la303924e.
[39] J. Liu, C. Dai, Y. Hu, Aqueous aggregation behavior of citric acid coated magnetite nanoparticles: Effects of pH, cations, anions, and humic acid, Environ. Res. 161 (2018) 49–60, https://doi.org/10.1016/j.envres.2017.10.045.
[40] M.M.M. Bindes, V.L. Cardoso, M.H.M. Reis, D.C. Boffito, Maximisation of the polyphenols extraction yield from green tea leaves and sequential clarification, J. Food Eng. 241 (2019) 97–104, https://doi.org/10.1016/j.jfoodeng.2018.08.006.
[41] Q. Hu, N. Chen, C. Feng, W.W. Hu, Nitrate adsorption from aqueous solution using granular chitosan-Fe 3+ complex, Appl. Surf. Sci. 347 (2015) 1–9, https://doi.org/10.1016/j.apsusc.2015.04.049.
[42] A. kheradmand, M. Negarestani, S. Kazemi, H. Shayesteh, S. Javanshir, H. Ghiasinejad, E. Jamshidi, Design and preparation magnetic bio-surfactant rhamnolipid-layered double hydroxide nanocomposite as an efficient and recyclable adsorbent for the removal of Rifampin from aqueous solution, Sep Purif Technol. 304 (2023) 122362. https://doi.org/10.1016/j.seppur.2022.122362.
[43] G.N. Doku, W.K. Agbozo, S.J. Haswell, T. McCreedy, Phosphomolybdenum Blue Detection – A Review of Characteristics, Achievements, Challenges and Future Prospects, Ghana Journal of, Science 61 (2020) 43–49, https://doi.org/10.4314/gjs.v61i1.4.
[44] Å. Kolmert, P. Wikström, K.B. Hallberg, A fast and simple turbidimetric method for the determination of sulfate in sulfate-reducing bacterial cultures, J. Microbiol. Methods 41 (2000) 179–184, https://doi.org/10.1016/S0167-7012(00)00154-8.
[45] G. William, Walter, Standard Methods For The examination of water and wastewater (11th ed.), WEF, 1961. https://doi.org/10.2105/ajph.51.6.940-a.
[46] D. Cao, X. Jin, L. Gan, T. Wang, Z. Chen, Chemosphere Removal of phosphate using iron oxide nanoparticles synthesized by eucalyptus leaf extract in the presence of CTAB surfactant, Chemosphere 159 (2016) 23–31, https://doi.org/10.1016/j.chemosphere.2016.05.080.

[47] Z. Wang, Iron complex nanoparticles synthesized by eucalyptus leaves, ACS Sustain. Chem. Eng. 1 (2013) 1551–1554, https://doi.org/10.1021/sc400174a.
[48] S. Bhattacharjee, DLS and zeta potential - What they are and what they are not?, J Control. Release 235 (2016) 337–351, https://doi.org/10.1016/j.jconrel.2016.06.017.
[49] H. Qiao, L. Mei, G. Chen, H. Liu, C. Peng, F. Ke, R. Hou, X. Wan, H. Cai, Adsorption of nitrate and phosphate from aqueous solution using amine cross-linked tea wastes, Appl. Surf. Sci. 483 (2019) 114–122, https://doi.org/10.1016/j.apsusc.2019.03.147.
[50] T. Iida, Y. Amano, M. Machida, F. Imazeki, Effect of Surface Property of Activated Carbon on Adsorption of Nitrate Ion, 61 (2013) 1173–1177
[51] N.Y. Acelas, C. Hadad, A. Restrepo, C. Ibarguen, E. Flórez, Adsorption of Nitrate and Bicarbonate on Fe-(Hydr)oxide, Inorg. Chem. 56 (2017) 5455–5464, https://doi.org/10.1021/acs.inorgchem.7b00513.
[52] H. Wang, X. Zhao, X. Han, Z. Tang, S. Liu, W. Guo, C. Deng, Q. Guo, H. Wang, F. Wu, X. Meng, J.P. Giesy, Effects of monovalent and divalent metal cations on the aggregation and suspension of Fe3O4 magnetic nanoparticles in aqueous solution, Sci. Total Environ. 586 (2017) 817–826, https://doi.org/10.1016/j.scitotenv.2017.02.060.
[53] R. Smernik, Environ. Soil Chem. (2003), https://doi.org/10.1016/s0167-8809(03)00222-6.
[54] E. Tombácz, I.Y. Tóth, D. Nesztor, E. Illés, A. Hajdú, M. Szekeres, L. Vékás, Adsorption of organic acids on magnetite nanoparticles, pH-dependent colloidal stability and salt tolerance, Colloids Surf. A Physicochem. Eng. Asp. 435 (2013) 91–96, https://doi.org/10.1016/j.colsurfa.2013.01.023.
[55] M. Li, J. Liu, Y. Xu, G. Qian, Phosphate adsorption on metal oxides and metal hydroxides: A comparative review, Environ. Rev. 24 (2016) 319–332, https://doi.org/10.1139/er-2015-0080.
[56] C. Spiteri, P. van Cappellen, P. Regnier, Surface complexation effects on phosphate adsorption to ferric iron oxyhydroxides along pH and salinity gradients in estuaries and coastal aquifers, Geochim. Cosmochim. Acta 72 (2008) 3431–3445, https://doi.org/10.1016/j.gca.2008.05.003.
[57] D.A. Almasri, N.B. Saleh, M.A. Atieh, G. McKay, S. Ahzi, Adsorption of phosphate on iron oxide doped halloysite nanotubes, Sci. Rep. 9 (2019) 1–13, https://doi.org/10.1038/s41598-019-39035-2.
[58] J. Lǔ, H. Liu, R. Liu, X. Zhao, L. Sun, J. Qu, Adsorptive removal of phosphate by a nanostructured Fe-Al-Mn trimetal oxide adsorbent, Powder Technol. 233 (2013) 146–154, https://doi.org/10.1016/j.powtec.2012.08.024.
[59] W. Gu, X. Li, M. Xing, W. Fang, D. Wu, Removal of phosphate from water by amine-functionalized copper ferrite chelated with La(III), Sci. Total Environ. 619–620 (2018) 42–48, https://doi.org/10.1016/j.scitotenv.2017.11.098.